International Journal of Nanoelectronics and Materials
Volume 16 (Special Issue) December 2023 [267-280]

Phase Reduction and Thermodynamic Analysis of Ilmenite Ore by Carbothermal-Iodination using Different Carbon Reductants

N. A. Nasrun[1], N. F. M. Yunos[2,3,*], M. A. Idris[1,3], S. R. R. Munusamy[1,3], N. Takahiro[4] and S. A. Rezan[5]

[1]Faculty of Chemical Engineering & Technology, Universiti Malaysia Perlis (UniMAP), 02600 Arau, Perlis, Malaysia
2Faculty of Mechanical Engineering & Technology, Universiti Malysia Perlis (UniMAP), 02600 Arau, Perlis, Malaysia
[3]Frontier Materials Research, Centre of Excellence (FrontMate), Universiti Malaysia Perlis (UniMAP), 01000 Kangar, Perlis, Malaysia
[4]Centre for Advanced Research of Energy and Materials, Hokkaido University, Kita 13 Nishi 8 Kita-Ku Sapporo 060-8628, Japan
[5]School of Materials and Mineral Resources Engineering, Universiti Sains Malaysia, Engineering Campus, Malaysia

ABSTRACT

The present study is on the combination of carbothermal reduction and iodination reaction (carboiodination) process for the phase reduction of ilmenite ore ($FeTiO_3$). The aim is to understand the phase reduction and thermodynamic reaction analysis of ilmenite ore by a combined method of carbothermal-iodination using different carbon reductants (graphite and palm char). Graphite was used as a standard carbon reductant while palm char as a renewable carbon reductant was prepared via the pyrolysis technique. Ilmenite was mixed with carbon reductants and then first reduced by using a carbothermal reduction process at 1550 ℃. Then, the reduced samples were further investigated with iodination reaction in different temperature ranges of 900-1000 °C using a vertical tube furnace with mixed argon and iodine gas (0.2 L/min). The proximate and ultimate analyses of carbon reductants were analysed by CHON analyser and their microstructure by using SEM, while XRF and XRD were used for analyzing the chemical compositions and the phase reductions of raw ilmenite ore and reduced samples, respectively. The thermodynamics of possible reactions during carbothermal-iodination reactions were calculated by HSC Chemistry 6.0 software. By comparing graphite and palm char, palm char had an amorphous structure, with porous and high carbon content showing high potential for usage as a reductant in titanium extraction from ilmenite ore. The phases of ilmenite ore were ilmenite, rutile, and anatase transformed into rutile, pseudobrookite, and titanium oxide detected by XRD. Further reduction was performed by palm char where more rutile (TiO_2) and titanium oxide (Ti_3O_5) developed from the iodination reaction at the highest temperature compared to graphite due to better properties and amorphous structure. The rutile and titanium oxide were found as stable phases from the thermodynamic analysis and confirmed with XRD. From the findings, the combination of carbothermal-iodination of ilmenite ore was possible and promising for rutile (TiO_2) production in mineral extractions.

Keywords: Phase reduction, carbothermal reduction, carboiodination reaction, palm char, graphite, thermodynamic analysis

1. INTRODUCTION

Currently, limited processing of pure synthetic rutile (TiO_2) gained the attention of researchers to extract rutile from ilmenite ore [1]. The leaching process using sulphate followed by ilmenite smelting in an electric furnace requires a high temperature of 1700℃ with longer processing times (8-10 hours). Salehi et al. discovered that temperature promotes the phase formation of

* Corresponding authors: farhanadiyana@unimap.edu.my

Ti_3O_5 at 1550°C. However, Ti_3O_5 formed into Ti_2O_3 and TiC in further reduction caused by the transportation of carbon to the surface of the oxide by dissolution in the carbon [2]. Investigation by He *et al*. on the pre-oxidation of ilmenite for 2 hours, followed by carbothermal reduction using coal and sodium carbonate additive at a temperature of 1500°C within 110 up to 160 minutes showed high production of titanium pentoxide and anatase [3]. Even though the production of Ti^3O^5 was high, however, this process required longer reaction times [4]. In order to increase the production of TiO^2 and Ti^3O^5, it was suggested to further use the halogenation process in a shorter time.

The halogenation process uses chlorine, bromine, and iodine to reduce ilmenite into rutile, Ti^3O^5, and the end product, titanium. The common halogenation process was the Kroll process [5]. However, due to the high production costs with a complex post-extraction procedure, these processes emitted a significant high quantity of carbon dioxide (CO^2). Several processes were used to replace the Kroll process [4] such as Ono Suzuki (OS)[6], FFC (Cambridge process)[6], and carboiodination[7]. Another study by Adipuri *et al*. on the carbothermal reduction at temperature of 1250°C followed by chlorination at 400°C for 25 minutes produced phases of Ti^3O^5 and titanium suboxides (Ti^xO^y)[8]. The chlorination process usually assist in the transformation of ilmenite into Ti^3O^5 and Ti^2O^3 phases [9]. The carboiodination did not gain much attention due to iron iodide does not exist in a stable form and is unaffected to undergo hydrolysis compared to ferric chloride. Nevertheless, when compared to carbochlorination process, the carboiodination process was expected to reduce effectively at above 850°C [7]. This process was beneficial for the reduction of ilmenite into rutile and Ti^3O^5[10]. The carboiodination process was suggested as a replacement for carbochlorination and carbobromination processes due to its ability to shorten the reaction, and processing steps, less energy consuming, and more cost-effective process of titanium production. This process able to be a substitute for sulphate process, carbochlorination, and metallothermic reduction [7]. It was found that the carboiodination process successfully removed iron from the ilmenite at a temperature of 800 °C [10].

During the carbothermal reduction, it is necessary to understand the possible thermodynamic reaction for industrial practice (30°C-1000°C) [11]. The chemical reactions involved were divided into solid-solid reaction equation, Boudouard reaction equation and gas-solid reaction equations. Lu et al. examined that, the carbothermic reduction of ilmenite had an activation energy of 225 $kJmol^{-1}$ [12]. However, the thermodynamic software calculated the value of activation energy as 180 $kJmol^{-1}$. The impurities in ilmenite such as Mn, SiO_2, and MgO were affecting the solid-solid and solid-gas reaction activation energy [13]. The benefits of thermochemical reaction calculation on high-grade ore ilmenite were to predict the thermal reaction and estimation of phase stability. Basically, the equilibrium model usually uses Factsage 8.2 and HSC Chemistry software [3]. Subasinghe *et al*. found that Equations (1) and (2) occurred with positive Gibb's energy and log K<0 within temperature 0°C-600°C [14]. However, log K>0 when the temperature was above 600°C indicated that the reaction experienced spontaneously. In addition, Equation (2) occurred nonspontaneous at temperatures ranging from 0 - 500°C while spontaneous reaction happened when the temperature was beyond 500°C (ΔG<0, K>0). The Equations (1), (2), and (3) became optimum when reached 1000°C with energy values of -116.320 $kJmol^{-1}$, -52.268 $kJmol^{-1}$ and -64.052 $kJmol^{-1}$ respectively [13].

Boudouard reaction

$$CO_{2(g)} + C \rightarrow 2CO_{(g)} \quad (1)$$
$$\Delta G = 167744 - 52.268\ J/mol$$

Solid-solid interaction

$$FeTiO_{3(s)} + C_{(s)} \rightarrow Fe_{(s)} + TiO_{2(s)} + CO_{(g)} \quad (2)$$
$$\Delta G = 311012 - 116.320\ J/mol$$

Gas-solid interaction

$$FeTiO_{3(s)} + CO_{(g)} \rightarrow Fe_{(s)} + TiO_{2(s)} + CO_{2(g)} \quad (3)$$

$$\Delta G = 143.268 - 64.052 \text{ J/mol}$$

The reduction process of ilmenite into rutile and titanium suboxides using biomass as a carbon reductant was advantageous. Koskela *et al*. found that non-renewable carbon reductants such as coal or coke, released pollutant gases that cause environmental pollution [15]. It was discovered that using biomass instead of coal and coke decreased CO2 emissions by about one-third and produced more metallic iron [16]. Waste biomass with low ash content and high carbon contents was used as biochar in ironmaking and mineral extractions [17, 18]. Mohammed *et al*., used palm char in carbothermal reduction at 1400°C. He found that palm char successfully reduced ilmenite into iron, titanium carbide, iron titania, titanium suboxides, and titanium dioxide [19]. This was due to the porous structure of palm char that enhanced the gas passed by the solid phase in carbothermal reduction [17]. The thermochemical decomposition of biomass via pyrolysis produced high carbon content at low temperatures (300-500°C) [16]. Some experimental studies focused on different parameters for pyrolysis such as temperature, flow rate, and residence time for carbon reductant in ironmaking and mineral extractions [16-18]. Yunos *et al*. investigated the reduction of palm char with the Langkawi ilmenite ore phase at various reaction durations (2-4 hours) and discovered that the phases changed to produce TiO_2, Fe, FeO, and TiC [17]. In other research, at the highest reduction temperature of 1400°C, the ilmenite ore phase was transformed into iron titania, titanium carbide, titanium dioxide, and iron [20].

Although a number of studies have been done on the phase reduction of ilmenite ore using carbothermal reduction, there are limited studies on the combination methods of carbothermal reduction and carboiodination reaction of ilmenite ore. This research aimed to investigate the phase reduction of ilmenite ore during carbothermal reduction at 1550°C and carboiodination reaction at temperatures 900- 1000°C for 30 minutes using different carbon reductants with thermodynamics calculation analysis using HSC Chemistry software to understand the possible chemical reactions that occurred with the reduction phases developed. In addition, the effect of different carbon reductants was investigated and discussed in detail to understand the carbon properties that contribute towards the reduction performance.

2. MATERIAL AND METHODS

2.1 Materials Preparation

This study consisted of combining two methods; carbothermal reduction and iodination reaction. The ilmenite ore was collected from Kinta Valley, Perak, Malaysia. The ilmenite ore was air dried for 24 hours to remove the moisture. Then, the ilmenite ore was milled by a ball mill machine and sieved to obtain particle size of <63µm. Two different carbon reductants which were graphite as a reference carbon reductant and palm shell was dried to remove moisture and crushed into a size of ~2mm. Then, the palm shell is converted into palm char via pyrolysis under nitrogen gas flow for 2 hours soaking time at 450 °C [17]. After that, all carbon reductants were milled and sieved into <63µm size. Finally, the sieved product (palm char and ilmenite) was mixed according to the carbon and oxygen molar ratio (1:3), while graphite and ilmenite were mixed into the ratio (1:6) as per stoichiometric calculations and palletized (weight 2 g) using a handpress with pressure of 100 MPa for 2 minutes.

2.2 Carbothermal Reduction Setup

The carbothermal reduction experiments were carried out in a horizontal tube furnace (TF42-1650 model) with closed-end tubes (Figure 1). The argon gas flowed into the furnace at 0.1 L/min to prevent reoxidation. The temperature was set at 1550 °C with a heating rate of 10 °C/min. The pellet mixture was placed inside the crucible in the hot zone of the furnace at an elevated temperature for 20 minutes, and then the reduced samples were collected to further the iodination reaction process.

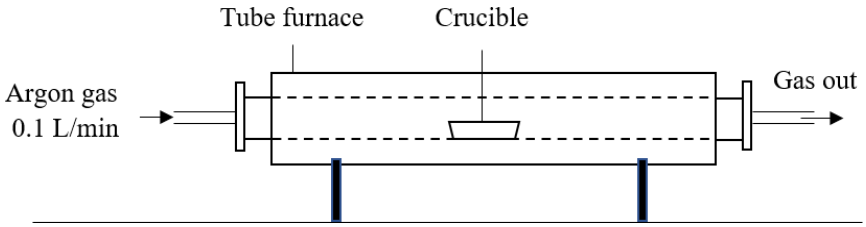

Figure 1. Carbothermal reduction setup.

2.3 Carboiodination Reaction Setup

The carboiodination experiment was carried out in a vertical quartz furnace with closed-end tubes (Figure 2). The tube was half filled with glass wool to place the samples in the hot zone. The reacting flask was put above the reacting flask at a temperature of 184°C to convert iodine liquid into iodine gas. The iodine gas flowed into a vertical furnace with the argon gas with a flow rate of 0.2 L/min. The other end of the vertical furnace connects with an empty reacting flask to capture the moisture and prevent the loop back of moisture to the furnace.

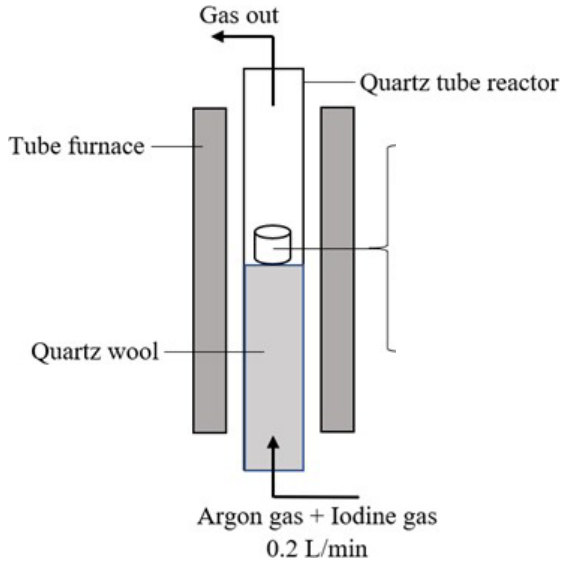

Figure 2. Carboiodination setup.

2.4 Sample Characterisations

The chemical compositions of the ilmenite ore, palm char, and graphite were determined by an X-ray Fluorescence (XRF) while the CHONS elemental analyser (Vario MACRO – Elementar) was used to investigate the carbon, hydrogen, oxygen, nitrogen, and sulfur content of carbon reductants according to ASTM D4442-92 [20]. The morphological structure and surface area of carbon reductants were examined by Scanning Electron Microscopy (SEM) and BET surface area, respectively.

X-ray Diffraction (XRD) was used to investigate the phase reduction during carbothermal reduction and carboiodination of ilmenite ore. The XRD model used was Benchtop Bruker D2 Phaser diffractometer with CuK-α, scanning rate 1s/step at 2□ range of 10°-90°. The interpretation of XRD data was analysed using X'Pert HighScore Plus 3.0e (3.0.5) Software. To evaluate the crystallinity of samples, Origin Pro2019b software was used to identify the crystalline and amorphous regions. The first step involved was to subtract the background that may be due to air scattering, noise, and unwanted signals. Next, the background curvature was adjusted before the amorphous area was calculated. The crystallinity can be computed using the formula given in Equation (4):

$$\%Amorphous = \frac{Total\ Area - Reduced\ Area\ (Amorphous)}{Diffractogram\ Total\ Are}$$

$$\%Crystallinity = 100 - \%Amorphous \quad (4)$$

The HSC Chemistry software 6.0 was used to calculate the free Gibbs energy and identify the thermodynamic chemical reactions that occurred in carbothermal reduction and carboiodination reaction at temperature ranges from room temperature up to 1000 °C based on the phase reduced in XRD analysis.

3. RESULTS AND DISCUSSION

3.1 Material Characterisations

The ilmenite ore, graphite, palm char, and raw palm shell were characterized by using XRF analysis. As shown in Table 1, the chemical composition of ilmenite ore consisted of 71.27 wt% TiO_2, 18.85 wt% Fe_2O_3, 2.72 wt% SiO_2, while other impurities were below 0.5 wt%. From the result, the grade of the ilmenite ore was considered as a high-grade ore where the TiO_2 content was above 55 wt% [21]. From Table 1, the major chemical composition of palm shells was mainly comprised of SiO_2 (22.77 wt%) and Fe_2O_3 (58.00 wt%) due to the nature of soil and fertilizer on the palm tree [21]. Other oxides found in raw palm shell were TiO_2 (0.73 wt%), Na_2O (1.55 wt%), MgO (1.60 wt%), Al_2O_3 (9.35 wt%), P_2O_5 (0.16 wt%), SO_3 (0.18 wt%), K_2O (3.45 wt%) and CaO (1.74 wt%). On the other hand, after pyrolysis, the palm shells were converted into palm char showing an increasing in SiO_2 percentage from 22.77 wt% up to 37.90 wt%. This was due to the oxygen and volatile portion being removed and affected by the pyrolysis temperature [16, 21]. According to XRF result for graphite, the highest oxide percentage was Al_2O_3 (38.44 wt%) and the lowest percentage was TiO_2 (0.13 wt%). It was found that the percentage of SiO_2 and CaO content of graphite was lower than palm char which made the graphite less impurities. However, the halogenation reaction was very sensitive to impurities such as CaO and MgO [22]. From the result, palm char had a low percentage of MgO compared to graphite which makes palm char more suitable to be carbon reductant in carboiodination of ilmenite [23].

Table 2 shows the ultimate and proximate analysis of graphite, palm shell, and palm char. Standard carbon reductant, graphite had a high carbon content of 98.1 wt%, while the carbon percentage of palm shells increased from 40.30 wt.% to 75.72 wt% after thermochemical conversion via pyrolysis. From the results, the carbon from palm char met the standard as activated carbon that contained high carbon >70 wt% that was suitable as carbon reductant with high product yield [24, 25]. At higher temperatures, the carbon content increased due to pyrolysis. The hydrogen, nitrogen, and oxygen contents were able to break the weaker bonds (e.g. carboxyl, hydroxyl) present in the palm shell structure at high temperatures [18]. The product of palm char showed the desirable properties of rich-carbon content, with low volatile and oxygen, that classified as high resistance to chemical reactions such as hydrolysis and oxidation. Palm char moisture showed a composition of 4.10 wt% that met also the standard of carbon reductants where the moisture ranged between 3.1 - 5.8 wt%. The moisture in palm char forms in a mineralized aqueous solution that contains cations, anions, and non-charged species. These properties delayed the removal of volatile matter during carbothermal reductions [26].

Table 1 Chemical composition of Perak's ilmenite ore, palm shell, palm char, and graphite by XRF analysis

Composition (wt %)	TiO_2	Fe_2O_3	Na_2O_3	MgO	Al_2O_3	SiO_2	P_2O_5	SO_3	K_2O	CaO
Ilmenite ore	71.27	18.85	0.39	0.64	-	2.72	0.13	0.03	0.12	0.10
Palm shell	0.73	58.00	1.55	1.60	9.36	22.77	0.16	0.18	3.45	1.74
Palm char	2.46	35.93	1.02	-	10.83	37.90	0.24	0.13	7.04	3.78
Graphite	0.13	5.17	12.92	26.61	38.44	6.32	0.19	3.32	0.64	1.06
- = non-detected										

The ash content of palm shell decreased from 24.30 down to 7.30 wt% (Table 2). The low content of ash in palm char hindered the blockage of the active site of carbon particles with ilmenite during carboiodination. Carbon, hydrogen, and oxygen are the primary constituents of biomass. Palm char comprised of high carbon with high oxygen content and low sulphur (Table 2). Low sulphur can further improve the quality of charcoal as a reductant. Moreover, the high volatile (10.90wt%) and hydrogen (3.18wt%) contents in palm char compared to graphite could help in accelerating the reduction performance. Hydrogen in the form of carbohydrates, and palm shell (agricultural waste) can further be decomposed to produce CO and H_2 during thermal decomposition. Then, the reducing gases reduced the iron oxide into metallic iron and ilmenite into titanium suboxides [27].

Table 2 also demonstrates the BET surface area value for all carbon reductants. The BET surface area of graphite was reported to be 8.3767 m^2/g, a higher value than raw palm shells (4.0956 m^2/g) but lower than palm char (319.8212 m^2/g). The higher BET surface area of the palm char indicated the more porous structures of char compared to the graphite. According to Ueda et al., the higher surface area of biomass char was attributed to the treatment process, and a faster gasification reaction rate of the char was reported due to high reactivity [28]. These porous structures led to high reduction performance [29].

Table 2 The ultimate and proximate analysis with BET surface area values of carbon reductants (graphite, palm shell, and palm char)

Ultimate analysis				**Proximate analysis**			
Composition (wt%)	**Graphite**	**Palm Shell**	**Palm Char**	**Composition (wt%)**	**Graphite**	**Palm Shell**	**Palm Char**
Carbon	98.1	40.30	75.72	**Moisture**	-	6.60	4.10
Hydrogen	0.13	2.59	3.18	**Ash**	5.70	24.30	7.30
Nitrogen	-	0.45	0.81	**Volatile matter**	0.70	17.30	10.90
Sulphur	-	0.22	0.18	**Fixed carbon**	97.80	42.40	75.40
Oxygen	-	56.44	20.11	**Surface area (m^2/g)**	8.3767	4.0956	319.8212

The SEM micrographs of palm shell and palm char that resulted from the pyrolysis process at temperature 450 °C are shown in Figure 3 (a) and (b) respectively. Raw palm shells had a hexagonal structure with small pores on the surface. Figure 3(b) shows the progressive destruction of the cell wall of a hexagonal structure and wall rupture during pyrolysis with a porous structure. The opening wide pores were consistent with the surface area measurement as

in Table 2. The orderly pore development might be due to less tar and other impurities that clogged up the pores. The volatile removal caused the removal of the cell walls and wider pore structure [23]. On the other hand, graphite (Figure 3(c)) had a spheroidal surface type (rosette structure) and sheet-like structure while ilmenite structure (Figure 3(d)) was irregularly shaped due to the different chemical composition and impurities. It is well known that, for the low-grade ilmenite basically in the form of a lamellar-shaped and flaky-like structure [30]. However, Kinta Valley ilmenite was irregularly shaped. Thus, in the present study, the ilmenite was confirmed and categorized as high-grade ore (Table 1).

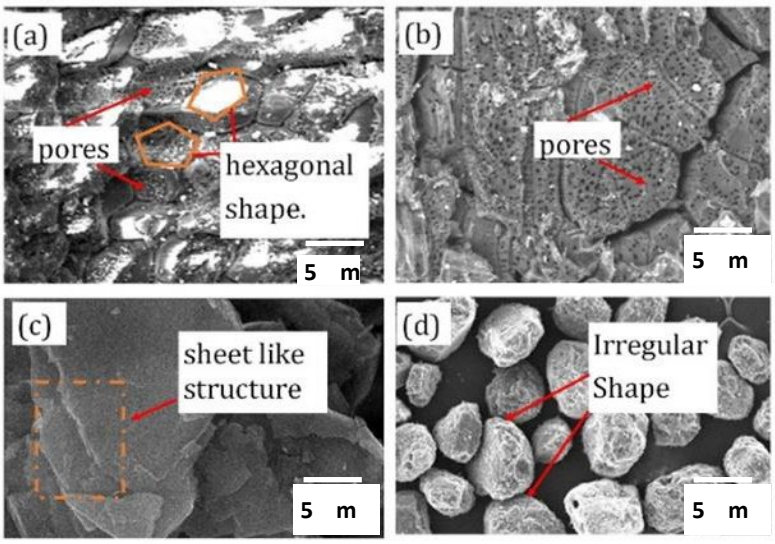

Figure 3. SEM Micrographs (a) Palm shell, (b) Palm char, (c) Graphite structure, (d) Ilmenite structure.

Figure 4 (a) and (b) display the XRD pattern of the carbon reductants. From the XRD pattern of raw palm shells, a broad peak at 2θ = 18−25° and a few small intense peaks at 2θ=30−54° indicated the presence of both amorphous and crystalline structures accordingly (Figure 4 (a)). For palm char, broad peaks were observed at around 2θ = 26° which corresponded to the peak of graphite. It is assigned to the planes of microcrystalline acknowledged as being turbostratic graphite structure on (002) [31]. According to Kurosaki *et al*., the pyrolytic reaction resulted in the breaking of chemical bonds and re-polymerization into active compounds [32]. Consequently, the compounds formed a graphitic layer and stacks of planes during pyrolysis. The appearance of two broad peaks in the XRD pattern suggested that the carbon structure was amorphous and had the asymmetric feature of the (002) peak of graphite. The presence of amorphous structure is caused by the breakage of C–C multiple bonds (primarily aromatic rings) in the raw palm shells and is associated with the formation of functional groups on the surface [31].

Phase analysis of graphite was shown in Figure 4 (b) with carbon peaks detected at angles of 26.44°, 44.52°, and 54.66°. The crystal system of graphite is hexagonal with 194 space group numbers. The XRD graph showed the graphitic structure with highly ordered material with carbon atoms organized by 6-unit cells that are interconnected towards adjacent cells from the combination of form planes [31]. Graphite consisted of a crystalline structure compared to palm char which both had crystalline and amorphous structures.

The degree of crystallinity (Table 3) calculated by Origin Lab software indicated that the palm shell comprised of 23.39 % crystalline and 76.61% amorphous structure. After pyrolysis, the carbon structure of palm char increased the crystallinity up to 50.60 % due to the decomposition of the cellulose structure in the palm shell. The result was similar to the decomposition of raw oil palm shell (OPS) into hydro char [28]. As in Figure 4 (b), the graphite peak at 26.44° (002) plane showed a highly crystalline structure (98.00%). Graphite is associated with the development of a three-dimensional crystalline structure of graphitic carbon. It was found that the reductant contained an intermediate structure called turbostratic between graphite and amorphous structure contributing to the reduction performance compared to crystalline structure [17].

Table 3 Crystallinity of carbon reductants by XRD analysis

Sample	Crystallinity (%)	Amorphous (%)
Graphite	98.00	2.00
Palm Shell	23.39	76.61
Palm Char	50.60	49.40

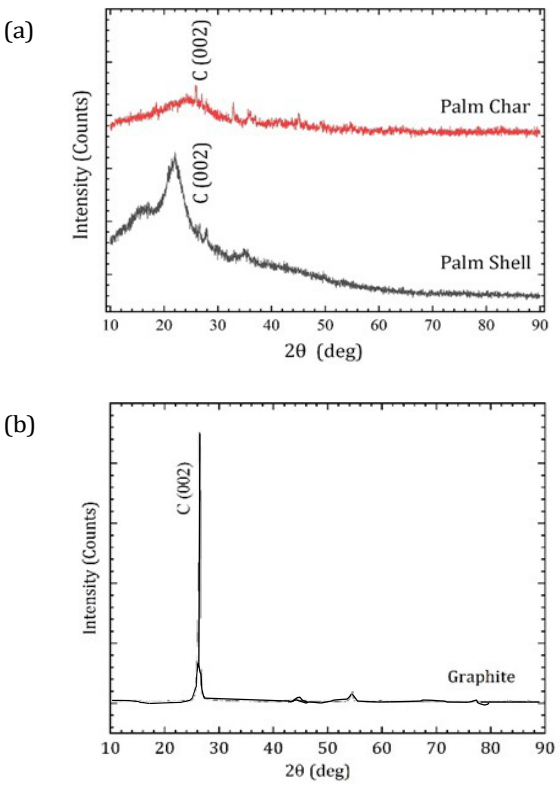

Figure 4. XRD analysis of carbon reductants (a) Palm shell & palm char (b) Graphite.

3.2 Phase Reduction of Ilmenite Ore After Carbothermal Reduction and Iodination Reactions

In Figure 5, the XRD analysis of ilmenite ore contained ilmenite ($FeTiO_3$) phases at angles 24.00°, 32.69°, 35.44°, 40.44°, 48.89°, 53.25°, 61.72° and 63.39°. The rutile (TiO_2) phases appeared at angles 27.62°, 36.32°, 41.48°, 54.47° and 70.10°. Anatase (TiO_2) phase in ilmenite ore was also detected at 2θ =27.5°. The reduced samples for different carbon reductants, palm char and graphite after carbothermal reduction also presented in Figure 5, showed the ilmenite phase was transformed into ilmenite, rutile, iron (Fe), titanium oxide (Ti_3O_5), and pseudobrookite (Fe_2TiO_5). From the figure, the anatase phase was completely transformed into rutile at high temperature reductions. The initial reduction of ilmenite ore into iron and rutile was the most rapid reaction and reasonably narrowed, indicating a high activation energy [33, 34]. The rutile phase developed from anatase and brookite phases during the carbothermal reduction of ilmenite ore at above temperature of 800 °C [35]. After carbothermal reduction, there was no titanium carbide, TiC phase was developed due to the high temperature selection in a short reaction time (20 mins). Terry et al. investigated on the carbothermal reduction of ilmenite ore at different temperatures (1300-1600 °C) and found that TiC phase developed above 1350 °C for 30 minutes of reaction time [36]. The final product became increasingly rich in Ti_3O_5 in 5 hours, while the titanium (III) oxide, Ti_2O_3 and TiC phases appeared after 1 hour reduction and the amount of this TiC phase was increased with time [36].

By comparing 2 carbon reductants, there was no Ti_3O_5 phase detected during the carbothermal process due to the formation of reverse transformation of pseudobrookite into ilmenite phase for palm char. The reverse chemical reaction transformation happened because the insufficient active site of carbon to hold oxygen was essential for the Boudouard reaction [37]. In addition, the high ash content (7.3 wt%) in Table 2 led to the blockage of the carbon active sites. Thus, carboiodination was needed for further process of reduction of ilmenite into more rutile production and Ti_3O_5 phases.

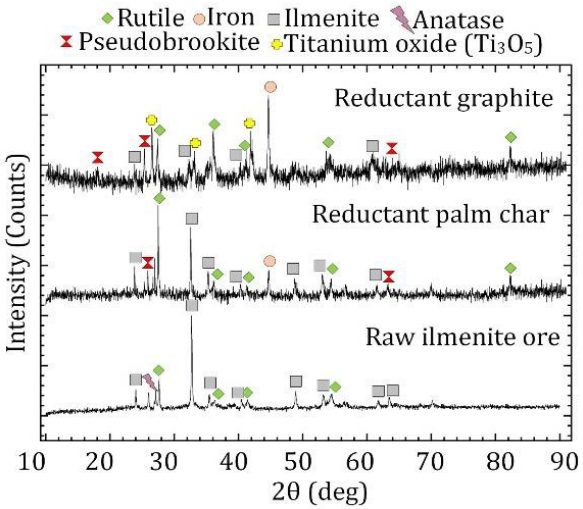

Figure 5. Phase reduction of ilmenite ore using graphite and palm char as carbon reductants by XRD analysis.

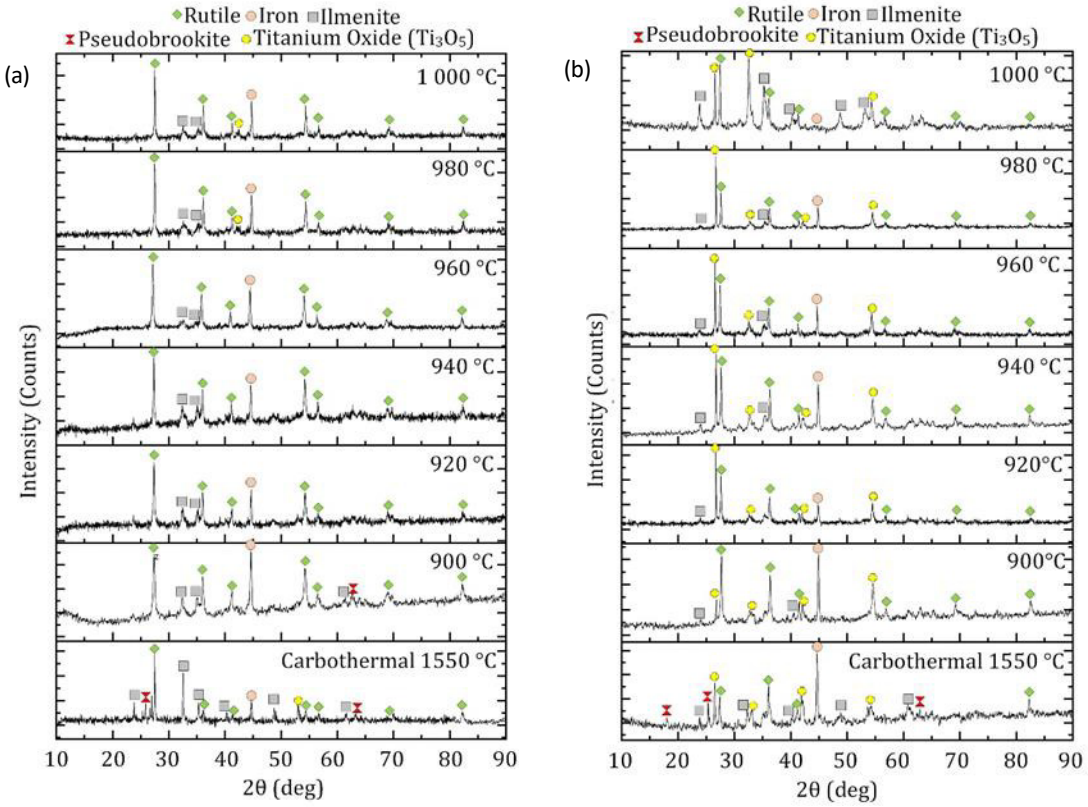

Figure 6. Phase reduction by XRD analysis of iodination reaction at different reduction temperatures of ilmenite after carbothermal reduction using different carbon reductants (a) Palm char (b) Graphite.

Further reduction from carbothermal reduction using iodination reaction at different reduction temperatures ranging from 900 up to 1000 °C process were investigated by XRD analysis as in Figure 6 (a) and (b). From Figure 6 (a), when palm char was injected as a carbon reductant, further reduction occurred. The phases of rutile, iron, pseudobrookite, and titanium oxide (Ti_3O_5) existed. The pseudobrookite phase appeared at an angle 48.85° at temperatures 900-940°C and none of the pseudobrookite phase developed at temperature 960-1000°C. More rutile phase was developed at temperatures 960-1000°C. The reduction of TiO_2 into Ti_3O_5 as in Figure 6(a) happened more feasible compared to graphite as in Figure 6(b) at 1000°C. From the results, it was beneficial to use graphite at lower temperatures since the intermediate phase pseudobrookite was fully converted into rutile. However, at 1000°C the phase of pseudobrookite appeared when using graphite as a carbon reductant. This was due to the lesser surface area and nonporous structure of graphite as in Table 2 and Figure 3, respectively. For palm char, the diffusion of gas through the layer of ash forms carbon monoxide promoted for carboiodination until 1000°C. The reduction phases changed from iodination reactions when palm char used as follows: $FeTi_2O_5$, Ti_3O_5, TiO_2, and Fe. As a result, the reduction performances of the amorphous and crystalline carbon structure of palm char were better than those of the crystalline carbon structure of graphite [28]. Additionally, for a greater degree of TiO_2 reduction, the high volatile matter content in carbonaceous materials was crucial in the release of gaseous reductants such as CO and CO_2 [38].

3.3 Thermodynamic Chemical Reaction of Carboiodination

According to the second rule of thermodynamics, the thermodynamic equilibrium of a chemical reaction in a closed system was estimated [12]. Figure 7 (a) and (b) showed the relationship between the ΔG and the temperature under different reduction temperatures. Based on the phase identified from XRD analysis in Figures 5 and 6, the following reduction reactions at 1550 °C were possible. From Figure 7 (a), it can be concluded that ΔG of Equations (2-10) in Table 4 for solid-solid reaction became more negative as the temperature increased and the driving force of the reduction reaction was enhanced by temperature (Equations 3, 5, and 6). Analysis based on Equations (8-11) shows that the reactions did not occur due to the positive ΔG value at the temperature ranges.

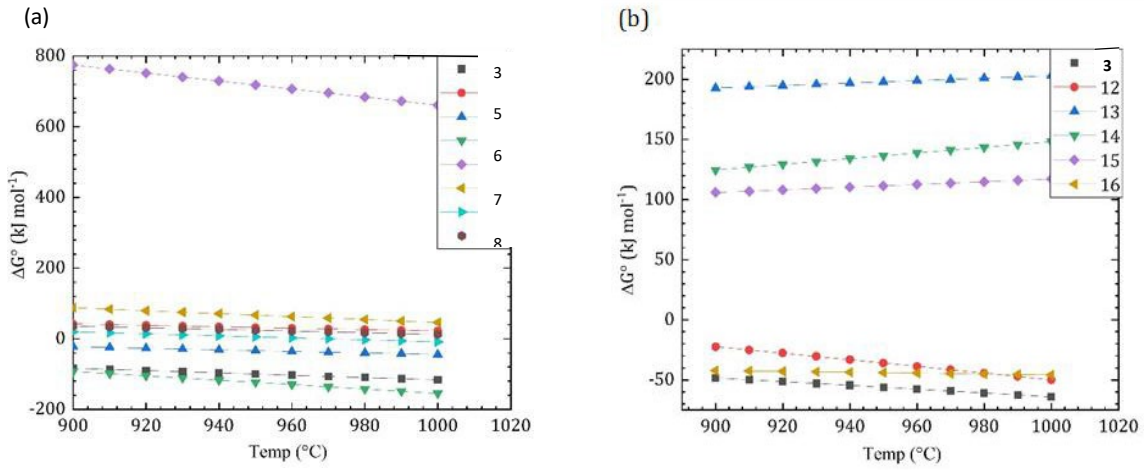

Figure 7. Thermodynamic plot of (a) Solid-solid reaction and (b) Gas-solid reaction.

The system dominant regions on $FeTiO_3$-TiO_2-Ti_3O_5-TiI_4 system using the thermodynamic calculation from HSC 6.0 software were shown in Figure 7 (a) and (b). Meanwhile, Table 4 indicates the free Gibbs energy involved by reaction of the equations that may occur in carboiodination according to XRD phase diagram result (Figure 5). Equation (1) represents the reaction between carbon and carbon dioxide to produce carbon monoxide during the reduction

of $FeTiO_3$ to TiO_2. The solid-solid reaction presented by Equations (2 – 11). From Table 4, Equations (5) and (11) did not occur at temperatures 900-1000 °C. However, the decreasing trend proved that the reaction may occurred at higher temperatures [39]. The gas-solid reaction as in Equations (3, 12-15) while Equations (13 - 15) did not react at temperatures 900°C-1000°C however, produced at lower temperatures (400-500 °C) [36].

Table 4 Thermodynamic possible chemical reactions during carbothermal reduction and iodination reactions

Type of Reactions	Equation No.
Boudouard reaction $CO_{2(g)} + C \rightarrow 2CO_{(g)}$ ΔG = 167744 – 52.268 J/mol	(1)
Solid-solid interaction $FeTiO_{3(s)} + C_{(s)} \rightarrow Fe_{(s)} + TiO_{2(s)} + CO_{(g)}$ ΔG = 311012 – 116.320 J/mol	(2)
$3TiO_{2(s)} + C_{(s)} \rightarrow Ti_3O_{5(s)} + CO_{(g)}$ ΔG = 276287 + 22.147 J/mol	(5)
$2FeTiO_{3(s)} + C_{(s)} \rightarrow Fe_{(s)} + FeTi_2O_{5(s)} + CO_{(g)}$ ΔG = 242176 – 44.478 J/mol	(6)
$FeTi_2O_{5(s)} + 2C_{(s)} \rightarrow Fe_{(s)} + Ti_2O_{3(s)} + 2CO_{(g)}$ ΔG = 647815 – 154.463 J/mol	(7)
$FeTi_2O_{5(s)} + 3C_{(s)} \rightarrow Fe_{(s)} + 2TiO_{(g)} + 3CO_{(g)}$ ΔG = 964572 – 50.345 J/mol	(8)
$3TiO_{2(s)} + 2I_{2(g)} + 3C_{(s)} \rightarrow TiI_{4(g)} + Ti_2O_{3(s)} + 3CO_{(g)}$ ΔG = −1580011 – 1505.760 J/mol	(9)
$Ti_2O_{3(s)} + 3C_{(s)} + 4I_{2(g)} \rightarrow 2TiI_{4(g)} + 3CO_{(g)}$ ΔG = 350.282 – 8.638 J/mol	(10)
$TiO_{2(s)} + 2C_{(s)} + 2I_{2(g)} \rightarrow TiI_{4(g)} + 2CO_{(g)}$ ΔG = 309.124 + 12.531 J/mol	(11)
Gas-solid interaction $FeTiO_{3(s)} + CO_{(g)} \rightarrow Fe_{(s)} + TiO_{2(s)} + CO_{2(g)}$ ΔG = 143.268 – 64.052 J/mol	(3)
$FeTi_2O_{5(s)} + 2CO_{(g)} \rightarrow Fe_{(s)} + Ti_2O_{3(s)} + 2CO_{2(g)}$ ΔG = 312327 – 49.927 J/mol	(12)
$3TiO_{2(s)} + 2I_{2(g)} + 3CO_{(g)} \rightarrow TiI_{4(g)} + Ti_2O_{3(s)} + 3CO_{2(g)}$ ΔG = 73858 + 203.035 J/mol	(13)
$Ti_2O_{3(s)} + 3CO_{(g)} + 4I_{2(g)} \rightarrow 2TiI_{4(g)} + 3CO_{2(g)}$ ΔG = −198799 + 227.770 J/mol	(14)
$TiO_{2(s)} + 2CO_{(g)} + 2I_{2(g)} \rightarrow TiI_{4(g)} + 2CO_{2(g)}$ ΔG = −49.288 + 156.869 J/mol	(15)

Figure 8 represents the thermodynamic calculation from HSC Chemistry software to identify the phase stability or equilibrium composition of reaction at one atmosphere from temperatures 100-1000°C based on the mole fraction of relevant phases in a mixture of $FeTiO_3$, C, I_2 and Ar. The amount of species inserted in HSC software were similar with the mixed ratio of ilmenite with carbon as in Section 2.1. From the Figure 8, the final product from the carboiodination reaction showed that the, $FeTi_2O_5$, TiO_2, Ti_2O_3, and Ti_3O_5 were stable phase above temperature of 700 °C, while carbon continuously reduced and stabled to reached the equilibrium at 1000 °C. The stable phases showed that the calculation in Free Gibbs energy as well from the XRD analysis in Figures 5 and 6 were consistent. The reduction of ilmenite proceeded rapidly to form metallic iron and rutile [40]. The rutile was then reduced to the lower oxides in the form of (Ti_nO_{n-1}), culminating in a more stable oxides (Ti_3O_5 and Ti_2O_3) at 1000 °C. The presence of iodine enhance more oxides reduction in ilmenite ore into rutile and titanium suboxides [27].

From the findings, it was expected that the first stage of reduction produced pseudobrookite, iron and rutile. During the subsequent carboiodination reaction, a series of phases of the general formula Ti_nO_{2n-1}, were formed. This proceeded until the formation of Ti_3O_5 which was quite stable [39].

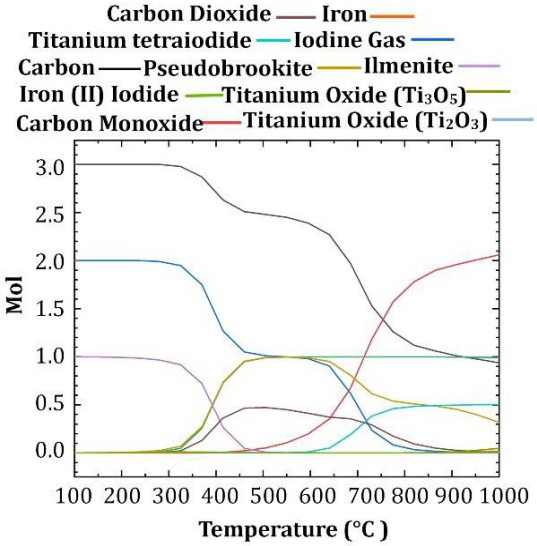

Figure 8. Equilibrium mol of carboiodination reaction.

4. CONCLUSIONS

From the findings, the combination of carbothermal reduction and carboiodination were beneficial to be used as an alternative method for extraction of rutile and titanium oxides from ilmenite ore by using palm char and graphite as reductant. From carbothermal reduction, the ilmenite phase was reduced into rutile, iron, pseudobrookite and titanium oxide. Following to further reduction by carboiodination reaction, the phase stabilizes into rutile and titanium oxide at highest temperature of 1000°C for both carbon reductant due to enough carbon for oxides removal. By using HSC calculation and estimation on the reaction during the process, the reaction products developed were consistent with the phase developed from XRD analysis. In addition, the palm char could be used as the alternative of carbon reductant due to excellent properties for carbothermal-iodination reduction method that could reduce the ilmenite ore into rutile and titanium oxide similar to graphite.

ACKNOWLEDGEMENTS

The authors acknowledge the financial support from the Fundamental Research Grant Scheme (FRGS) under Grant Number of FRGS/1/2020/TK0/UNIMAP/02/30 from the Ministry of Higher Education. The authors also acknowledge the support from Research Management and Innovation Center (RMIC), Faculty of Mechanical Engineering & Technology and Faculty of Chemical Engineering & Technology, Universiti Malaysia Perlis, (UniMAP) for this research.

REFERENCES

[1] Subasinghe, H. C. S. & A. S. Ratnayake. Minerals Eng. vol 173 (2021) pp. 107197.
[2] Salehi, H. *et al*., Mining, Metall. & Exploration, vol 38, issue 2 (2021) pp. 1167-1173.
[3] He, C. *et al*., Minerals, vol 11, issue 2 (2021) pp. 104.
[4] Berger, L. M., J. Mater. Sci. Lett., vol. 20, issue 20 (2001) pp. 1845-1848.

[5] Hu, D., Dolganov, A., Ma, M., Bhattacharya, B., Bishop, M. T., & G. Z. Chen, JOM, vol 70, issue 2 (2018) pp. 129-137.
[6] Nakamura, K., Iida, T., Nakamura, N., & Araike, T., Materials Transactions, vol 58, issue 3 (2017) pp. 319-321.
[7] Schlender, P. & Adam, A. E. W. Ind. Eng. Chem. Res., vol 56, issue 23 (2017) pp. 6572- 6578.
[8] A. Adipuri, Y. Li, G. Zhang, & O. Ostrovski, Int. J. Miner. Process., vol. 100, no. 3–4 (2011).
[9] Ahmadi, E., *et al.*, Metall. Mater. Trans. B Process Metall. Mater. Process. Sci., vol 48, issue 5 (2017) pp. 2354-2366.
[10] Singhania, A. & Bhaskarwar, A. N. Fuel, vol 221 (2018) pp. 393-398.
[11] Hu Chen, X., Wang, H., Min Liu, Y., & M. Fang, Trans. Nonferrous Met. Soc. China (English Ed., vol 19, issue 5 (2009).
[12] Dong Lu, X., Chen, D., Tao Xin, Y., *et al.*, Trans. Nonferrous Met. Soc. China (English Ed., vol. 32, issue 3 (2022).
[13] Zhang, G., H. Gou, K. Wu, & K. Chou, Vacuum, vol 143 (2017) pp. 199-208.
[14] Subasinghe, H. C. S. & Ratnayake, A. S., J. Alloys Compd., vol 954 (2023) pp. 170086.
[15] Koskela, A., Heikkilä, A., Bergna, D., J. Salminen, & T. Fabritius, Minerals, vol 11, issue 2 (2021) pp. 187.
[16] Yunos, N. F M., *et al*., J. Ther. Ana. and Calorimetry, vol 138 issue 1 (2019) pp. 175-183.
[17] Mohammed, A. I., *et al*., Chem. Eng. Res. Des., vol 178 (2022) pp. 583-589.
[18] Najmi, N. H., Yunos, N. F. M., Othman, N. K., & Idris, M. A., J. Mater. Res. Technol., vol 8, issue 2 (2019) pp. 1720-1728.
[19] Mohammed, A. I., *et al*., Int. J. Nanoelectron. Mater., vol 15 issue 1 (2022) pp. 1-8.
[20] Bhalla, A., Kucukkargoz, C. S. & Eric, R. H., J. South. African Inst. Min. Metall., vol 117, issue 5 (2017) pp. 415-421.
[21] Najmi, N. H., *et al*., Solid State Phenomena, vol 280 (2018) pp. 433-439.
[22] Ouellette, R. J. & Rawn, J. D., "Structure and Bonding in Organic Compounds," in Organic Chemistry (2018).
[23] Yunos, N. F. M., *et al*., J. Sustain. Metall., vol 7 issue 2 (2021) pp. 412-426.
[24] Fidalgo, B., Berrueco, C. & Millan, M., J. Anal. Appl. Pyrolysis, vol 113 (2015) pp. 274-280.
[25] Wang, G., *et al*., Int. J. of Min., Metall., and Materials, vol 25, issue 1(2015) pp. 28-36.
[26] Willner, T. & Brunner, G., Chem. Eng. Technol., vol 28, issue 10 (2005) pp. 1212-1225.
[27] Huang, R., *et al*., Metallurgist, vol 61, issue 5 (2017) pp. 511-516.
[28] Setiawan, A. *et al*., J. Sustain. Metall., vol 7, issue 4 (2021) pp. 1819-1837.
[29] Yunos, N. F. M., Chong, J. H., Mohamed, A. I., & M. A. Idris, Mat. Sc. Forum, vol. 1010 (2020) pp. 391-396.
[30] Sharifah, A. S. S., Saidin, H. S., Baharun, N., Rezan, S. A. & Hashim, H., Adv. Mat. Research, vol. 858 (2014) pp. 265-271.
[31] Barnakov, C. N., Khokhlova, G. P. V. Y. Malysheva, A. N. Popova, & Z. R. Ismagilov, Solid Fuel Chem., vol. 49, no. 1 (2015).
[32] Kurosaki, F. Ishimaru, K., Hata, T., Bronsveld, P., Kobayashi, E., & Imamura, Y., Carbon., vol 41 issue 15 (2003).
[33] Li, J.G. & Ishigaki, T., Acta Materialia, vol 52, issue 17(2004) pp. 5143-5150.
[34] Dewan, M. A. R. Zhang, G. Q. & Ostrovski, O., Trans. Institutions Min. Metall. Sect. C Miner. Process. Extr. Metall., vol 120 issue 2 (2011) pp. 111-117.
[35] Hanaor, D. A. H. & Sorrell, C.C., J. of Mat. Science, vol 46, issue 4 (2011) pp. 855-874.
[36] K. H. Wu, *et al*., J. Sol. State Chemistry, vol. 277 (2019) pp. 793-803.
[37] Gou, H.P., *et al*., Trans. of Nonferrous Metals Soc. China, vol 27, issue 8(2017) pp. 1856-1861.
[38] Peng Gou, H., Hua Zhang, G., Jun Hu, X. & Chih Chou, K. "Trans. Nonferrous Met. Soc. China (English Ed.), vol. 27, no. 8 (2017).
[39] Setiawan, A., *et al*., J. Sustainable Metall. vol 7, issue 4 (2021) pp. 1819-1837.
[40] Sri Harjanto, C. I. L., *et al*. Int. J. of Technology, vol. 12, issue 6 (2021) pp. 291-319.